JOURNAL OF GEOPHYSICAL RESEARCH, VOL. 99, NO. C9, PAGES 18,481–18,499, SEPTEMBER 15, 1994

Sensitivity of eddy-induced heat transport to diabatic forcing

Sybren S. Drijfhout
Royal Netherlands Meteorological Institute, De Bilt

Abstract. Compensation of the poleward eddy heat transport by the heat transport of an eddy-induced mean meridional overturning cell is a common feature in many eddy-resolving ocean models. It has been argued that this is the result of the weak thermal driving of the ocean. As the actual air/sea coupling is scale dependent, it might be questioned whether the approximation of weak thermal driving is relevant for the oceanic eddy field. In this paper the role of diabatic forcing in modifying eddy–mean flow interaction is investigated. Emphasis has been placed on the sensitivity of the eddy-induced change in heat transport to the sea surface thermal boundary condition. Experiments have been performed with a multilayer isopycnic primitive equation model of an idealized North Atlantic subtropical and subpolar gyre. For different values of the air/sea coupling, solutions with and without transient eddies have been compared. The air/sea coupling mostly affects the upper ocean thermal and velocity fields. A decrease of the coupling timescale pushes the separation point of the midlatitude jet further northward and induces a tight recirculation southwest of the separated jet. These effects are enhanced by the eddies. In the present model there is compensation of the eddy heat transport for sea surface temperature (SST) relaxation times longer than 150 days; a breakdown of the compensation occurs for SST relaxation times shorter than 50 days (the average upper layer depth is 200 m). In between is a transition regime. For strong thermal driving the eddy-induced change in total heat transport is of the same order as the eddy heat transport.

1. Introduction

The large-scale ocean circulation is driven by mechanical (wind) and thermohaline forcing. The latter forcing is basically an interactive process between ocean and atmosphere. The development of theories of the general circulation driven by buoyancy forces has been troubled by the difficulty that the stratification, which wind-driven theories treat as a priori known, has become an additional unknown.

A solution for the global ocean was given by *Veronis* [1978], who combined Ekman pumping distributions and a prescribed interior upwelling in a two-layer model. A different approach to explain the mid-ocean circulation was given by *Luyten et al.* [1983], who developed a multilayer model of the ventilated thermocline which provided for a theory in which both buoyancy and wind-forcing could be included. However, most studies that extended the model of Luyten et al. prescribe the density at the base of the mixed layer, which is more a circumvention of the air/sea interaction problem.

Pedlosky et al. [1984] and *Luyten and Stommel* [1986] addressed the influence of air/sea interaction on the ventilated thermocline. However, the former used a prescribed heat flux and the latter a prescribed mass exchange between the layers. *Cushman-Roisin* [1987] used a similar model with a Haney-type [*Haney*, 1971] forcing, in which the thermocline temperature is relaxed to prescribed values, combined with a heat exchange with the deep ocean. These studies have given us valuable insights, but suffer from limiting hypotheses, such as the neglect of inertial terms and friction. For this reason these models have only a regional validity as the solution for the "open ocean" is decoupled from the western boundary currents. To obtain a (thermo)dynamically closed system a numerical model seems advantageous.

Various numerical models of the wind- and buoyancy-driven ocean circulation have been designed to test aspects of the theory of the ventilated thermocline and to extend this theory [e.g., *Cox and Bryan*, 1984; *Huang and Bryan*, 1987; *Colin de Verdière*, 1989]. In most of these models, small-scale turbulence and ringlike eddies are parameterized in terms of diffusion and friction.

The effect of such parameterization on the overall ocean heat budget has been addressed by *Cox* [1985] and *Bryan* [1986], by comparing eddy-resolving and non-eddy-resolving versions of an ocean model. Due to a near compensation between the eddy heat transport and an eddy-induced change in heat transport by the mean flow, this parameterization was concluded to be valid with respect to the heat budget. *Bryan* [1986] argued that this compensation should be the result of the weak thermal driving of the ocean.

The higher-resolution study with the Cox model by *Böning and Budich* [1992] urged *Bryan* [1991] to readdress this issue. He concluded that both model versions show the same compensation mechanism. This compensation was the result of changes in the shallow meridional overturning cells that are related to the Ekman pumping, and these overturning anomalies should be related to changes in the zonal cross-basin pressure gradient. He also argued that the heat transport compensation was similar to the compensation found for stratospheric waves and suggested that the generalized Eliassen-Palm concept developed by *Andrews and McIntyre* [1976] should be a valuable framework for an explanation of this compensation.

Paper number 94JC01627.
0148-0227/94/94JC-01627$05.00

These ideas were further examined by *Drijfhout* [1994]. The robustness of the compensation phenomenon with respect to model formulation and degree of nonlinearity was tested, using an isopycnic model of the *Semtner and Mintz* [1977] basin, where the enhanced wind forcing secures a stronger midlatitude jet and eddy field. Results show that compensation of the eddy heat transport also occurs in this model configuration.

Furthermore, *Drijfhout* [1994] confirmed that the enhancement of the overturning is mainly associated with an eddy-induced change in zonal pressure gradient, brought about by a zonal eddy heat transport against the direction of the parent stream. In this model the mean flow forcing by the eddies was nearly balanced by an eddy-induced change in cross-basin zonal pressure gradient. This eddy–mean flow interaction principle secured the net non–heat transport character of the eddies.

It was shown that the strength of the atmosphere/ocean coupling should be essential in the determination of the eddy–mean flow interaction. The non–heat transport character of the eddies could only be demonstrated under weak diabatic forcing conditions. With respect to rings this implies that diabatic effects must be small during the period that they are isolated, and modification of their sea surface temperature (SST) anomalies should be negligible during their lifetime. It was hypothesized that the non–heat transport character of the eddies would break down when the diabatic forcing was enhanced.

The discussion on the critical role of diabatic effects by *Bryan* [1986, 1991] was extended by the introduction of a nondimensional parameter $\Gamma = L/(U\tau)$, where U is the wind-driven velocity, L is a representative length scale, and τ is the relaxation time of SST anomalies. This parameter indicates the relative importance of the diabatic forcing to advective changes in the heat equation. It effectively measures the ratio between the SST relaxation time and the advective timescale.

Huang [1989] demonstrated that Γ is a controlling factor in describing the thermodynamical air/sea coupling in a non-eddy-resolving ocean model. In that study the length scale L was determined by the scale of the gyre. It can be argued that the gyre circulation timescale should be the relevant timescale of the eddy field. For isolated eddies, modification of the air/sea heat exchange through their SST anomaly is operative while they are isolated from the mean flow. The lifetime of isolated eddies is typical of the order of the gyre circulation time, i.e., the time needed to bring them back to the western boundary current. On the other hand, one can argue that the length scale of the eddy field itself should be the relevant one [*Drijfhout*, 1994]. In the present study the ratio of the two length scales is constant, and we shall use Huang's definition of Γ in the remainder of the text.

Typical values of Γ suggest that the actual air/sea coupling should be intermediate in strength, varying between weak and strong (in general $0.1 < \Gamma < 10$, while the proper value of τ is unknown and, moreover, τ will be a function of the oceanic and atmospheric flow configuration). According to *Drijfhout* [1994], $\Gamma = 0.4$ (with the length scale L determined by the eddy field $\Gamma = 0.15$; in that paper Γ was calculated to be 0.3, as the scale of the wind field was erroneously multiplied by a factor of 2). Compensation of the eddy heat transport was the result of a rather weak thermal driving. It was shown that compensation occurs when diabatic effects are small compared to advective changes in the heat equation, i.e., when $\Gamma < 1$. It was suggested that compensation of the eddy heat transport might already break down for realistic values of the diabatic forcing, when Γ becomes of the order of one. Moreover, the coupling coefficient (inverse of the relaxation time for SST anomalies) is reduced by the feedback of SST anomalies to the atmospheric boundary layer temperature. However, such feedback on the ocean mesoscale should be negligible.

This suggests that in reality the coupling will be scale dependent; the coupling will be stronger for smaller-scale SST anomalies. Also the coupling will depend on the depth of the mixed layer and details of the flow field. It should be clear that the thermal forcing has to be varied over a wide range to be able to draw conclusions on the possible role of eddies in the ocean heat budget from simulations.

This study investigates the influence of the upper thermal boundary condition on eddy–mean flow interaction and the eddy-induced change in heat transport. *Drijfhout*'s [1994] model is used to find solutions for different Γ. In that study it was found that due to the relatively strong wind forcing and subsequent strong nonlinear flow field, there were no qualitative differences between a 1/3° × 1/3° and a 1/6° × 1/6° version of the model if weak biharmonic frictions were used: Already at 1/3° resolution the hydrodynamical instability of the flow is so strong that the eddy kinetic energy dominates the mean kinetic energy and ring formation is described. With strong Laplacian friction, however, the 1/3° × 1/3° resolution model generates no eddies, but attains a steady state after spin-up. Hence for reasons of computational efficiency in this study, solutions for strong Laplacian friction (without eddies) and weak biharmonic friction (with eddies) are compared on a 1/3° × 1/3° grid for a range of different Γ values.

The outline of the paper is as follows. A description of the numerical model is given in section 2. A comparison of mean flow fields with and without eddies for different Γ is given in section 3. The effect of Γ on the eddy-induced change in meridional heat transport is evaluated in section 4. In section 5 the eddy–mean flow interaction that causes a (partial) compensation of the poleward eddy heat transport is analyzed and the role of diabatic forcing in this eddy–mean flow interaction is described. In section 6 we summarize our findings and present our conclusions.

2. Description of the Numerical Model

In this section a short description is given of the numerical model. For more details we refer the reader to *Drijfhout* [1994]. The model consists of a three-layer primitive equation isopycnic model as described by *Bleck and Boudra* [1986]. The use of an isopycnic model to study the eddy heat transport was suggested by *Drijfhout* [1992]. Model domain and wind forcing are the same as those from *Semtner and Mintz* [1977] (Figure 1). The bottom topography mimics the continental slope beneath the western boundary current with a flat bottom outside this region. Apart from this slope the average layer depths are 200 m, 600 m, and 3400 m. The reduced gravities at the interfaces are respectively $g'_1 = 1.3 \times 10^{-2}$ m s^{-2} and $g'_2 = 0.7 \times 10^{-2}$ m s^{-2}, corresponding to a temperature difference between layers 1 and 2 of 6.5°C, and 3.5°C for layers 2 and 3.

The momentum equations of the model are

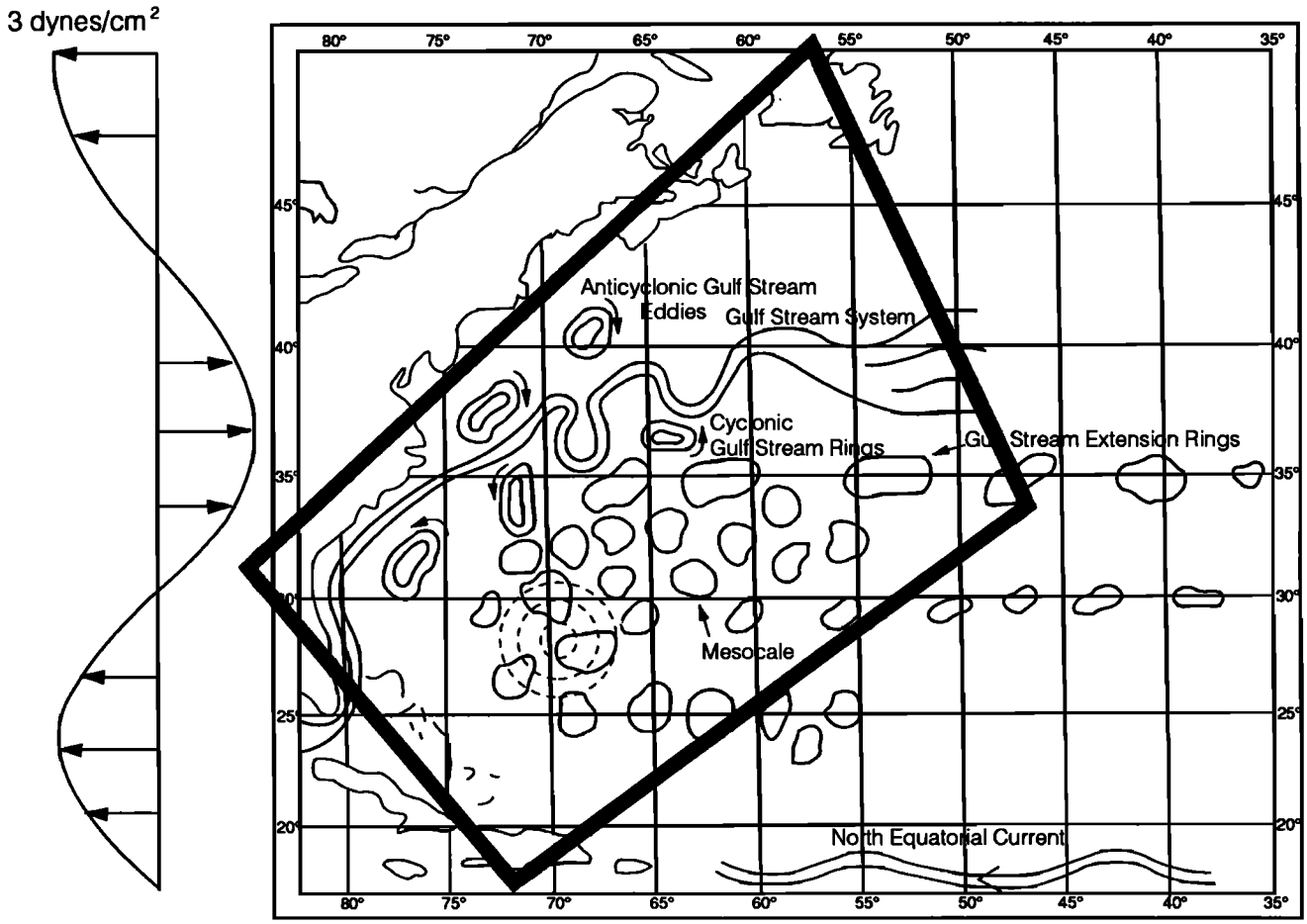

Figure 1. The boundary of the model domain, superimposed on a schematic picture of mesoscale variability in the western portion of the North Atlantic. Also shown is the zonal wind stress which drives the model ocean. The upper layer depth is relaxed to prescribed values which show a linear variation with latitude. Extreme values are −260 m at the northern tip and 660 m at the southern tip of the domain.

$$u_t + (\mathbf{u}^2/2)_x - (f+\zeta)v = -M_x - B_M\nabla^4 u + \frac{1}{\Delta h}(g\Delta\tau_x) \tag{1}$$

$$v_t + (\mathbf{u}^2/2)_y + (f+\zeta)u = -M_y - B_M\nabla^4 v + \frac{1}{\Delta h}(g\Delta\tau_y) \tag{2}$$

In these equations $\mathbf{u} = (u, v)$ is the horizontal velocity, f is the Coriolis parameter, $\zeta = v_x - u_y$ is the relative vorticity, $M = gz + p/\rho$ is the Montgomery potential, g is the gravity acceleration, p represents the pressure, Δh is the thickness of the isopycnic layer, $(\Delta\tau_x, \Delta\tau_y)$ are the wind- and bottom drag–related stress differences in the x and y direction between the top and bottom of a coordinate layer. The wind stress is assumed to decrease linearly within a layer of 100 m. If the surface layer(s) is (are) shallower than this value, part of the wind stress is passed to the layer below. A quadratic bottom stress is used. We assume that it decreases linearly within a layer of 10 m.

B_M is a viscosity parameter. (In some experiments the biharmonic friction is replaced by Laplacian friction: $A_M\nabla^2\mathbf{u}$). The lateral boundary condition for the velocity is a free-slip condition.

The hydrostatic equation reads

$$M_s = p\frac{\partial}{\partial s}(1/\rho) \tag{3}$$

where s is the vertical coordinate of the isopycnic model.

The equation for the layer thickness h reads

$$\frac{\partial}{\partial t}h + \nabla\cdot\mathbf{U} = -B_T\nabla^4 h + \gamma(h^* - h) \tag{4}$$

where $\mathbf{U}$ is the horizontal mass transport. (In some experiments $B_T\nabla^4 h$ has been replaced by a Laplacian friction $A_T\nabla^2 h$). The lateral boundary condition for the layer thickness is a no-flux condition. For the numerical formulation of the boundary conditions we refer the reader to *Semtner and Mintz* [1977].

The Haney forcing [*Haney*, 1971], $\partial T/\partial t = \gamma(T^* - T)$, is rewritten as $\partial h/\partial t = \gamma(h^* - h)$, where h^* must be interpreted as an equivalent apparent air temperature.

In the standard run of *Drijfhout* [1994] the coefficient γ times $\bar{h}$ is 0.6 m d^{-1}, the same value as that given by *Semtner and Mintz* [1977]. With an average upper layer depth of 200 m this is equivalent to a relaxation time for

Table 1. Parameter Values Used in Study of the Model's Sensitivity to the Diabatic Forcing

Run	Γ	τ_r
1	0.4	333
2	0.8	167
3	1.6	83
4	3.2	42
5	6.4	21
6	12.8	10

Here τ_r is the SST relaxation time.

surface thickness (temperature) anomalies of 333 days. In the next section this standard run is compared with solutions obtained for higher values of γ and subsequent smaller values for the relaxation time of SST anomalies.

3. Comparison of Solutions

The main topic of this study is the model's sensitivity to the relaxation time of SST anomalies as applied to the imposed Haney-type buoyancy forcing. *Drijfhout* [1994] described a run for weak thermal forcing, $\Gamma = 0.4$, where the strength of the thermal driving is expressed by the nondimensional parameter Γ, as suggested by *Huang* [1989]:

$$\Gamma = L/(U\tau) \tag{5}$$

where L is the length scale of the gyre, U is the wind-driven velocity, and τ is the relaxation time for the surface thermal field. The parameter Γ effectively measures the ratio of the circulation time of the wind-driven gyres to the relaxation time of the upper layer temperature field to the buoyancy forcing. The value for Γ of 0.4 corresponds to a relaxation time of 333 days for an upper layer with an average depth of 200 m. In the present study the effect of increasing Γ, i.e., a stronger thermal driving, has been explored to study how the eddy–mean flow interaction changes and whether eddy-induced changes in the overall heat transport occur for stronger thermal driving. Table 1 lists the various runs in order of the values used for Γ.

The spin-up of the model consists of several stages with various grid size and friction parameterizations (see *Drijfhout* [1994] for details). The first 30 years have been run with a coarse grid configuration, i.e., a horizontal resolution of 74 km (about 2/3° × 2/3°). Laplacian friction has been used, the viscosity parameter A_M is 10^3 m^2 s^{-1}, and the diffusivity parameter A_T is 0.5×10^3 m^2 s^{-1}. Thereafter the grid size is reduced to 37 km. Between years 30 and 40 the friction remains unchanged. The steady state attained is denoted experiment 1 for each run with a constant Γ. Due to the large Laplacian friction coefficients, there are no transient eddies present in the solution.

At year 40 the friction parameters are decreased, and a weak eddy field appears. After the model has reached a statistical equilibrium with the (weak) eddy field, we change from Laplacian friction to biharmonic friction; B_M is 10^{11} m^4 s^{-1}, B_T is 1.5×10^{11} m^4 s^{-1}. Now the flow field displays hydrodynamic instabilities. The model is integrated for another 15 years to attain a new statistical equilibrium with the strong eddy field. This equilibrium is called experiment 2 for each run.

The upper layer thickness field for the standard run of *Drijfhout* [1994] shows that in both experiments, with and without eddies, the imposed wind forcing drives a two and a half gyre circulation (Figure 2). A model counterpart of the

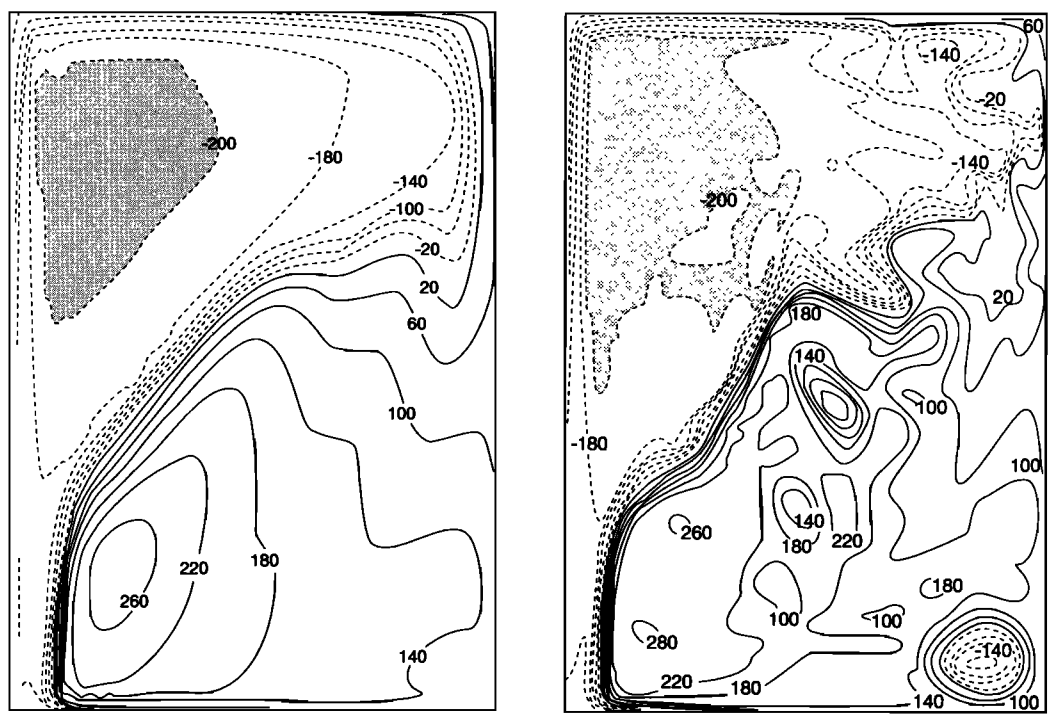

Figure 2. (Instantaneous) upper layer thickness fields for (left) experiment 1 and (right) experiment 2 for Γ = 0.4. Values are in meters relative to the average thickness of 200 m. Stippled areas denote a zero thickness (outcropping).

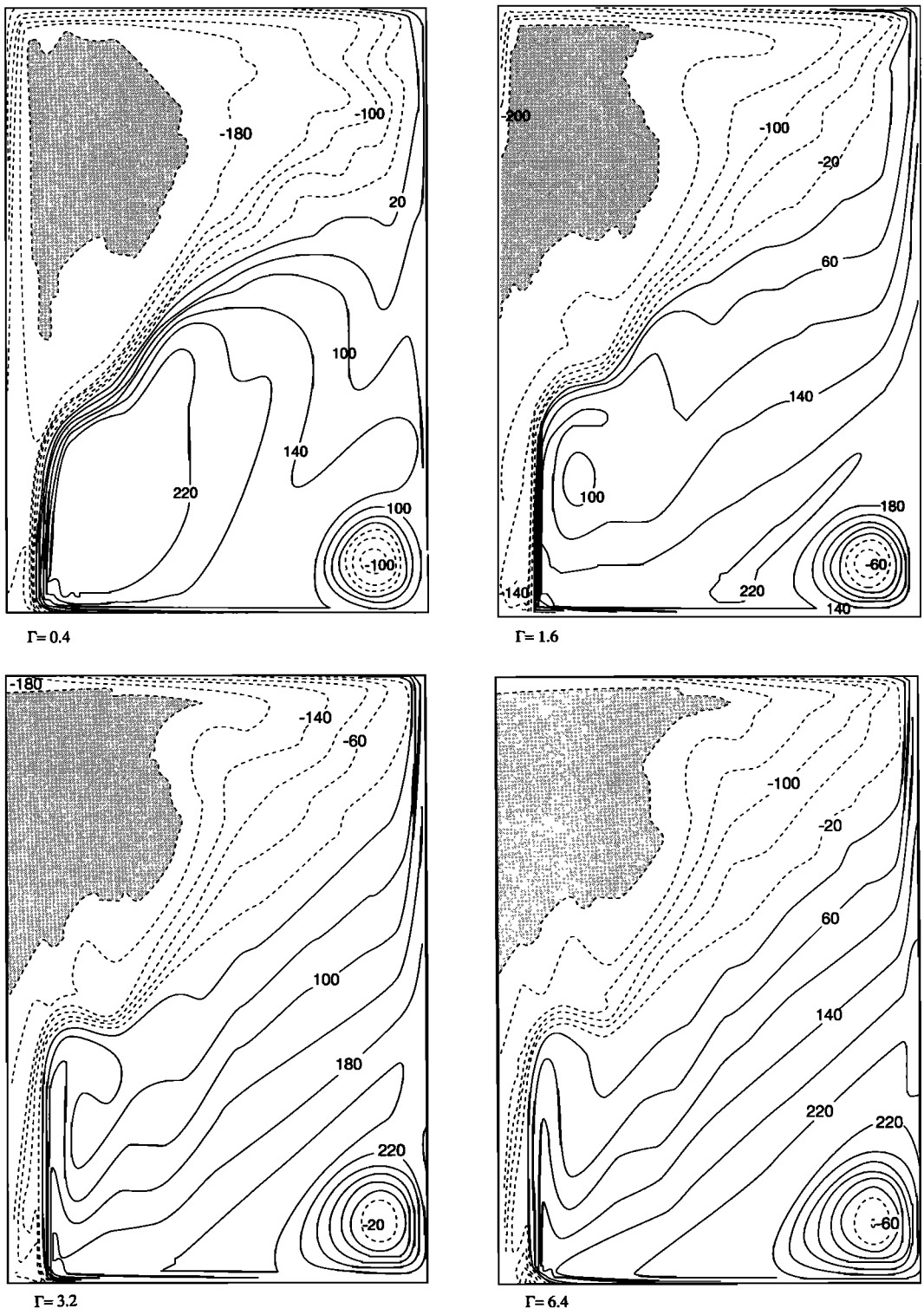

Figure 3. Time-averaged upper layer thickness fields for experiment 2, for $\Gamma = 0.4$ (top left), $\Gamma = 1.6$ (top right), $\Gamma = 3.2$ (bottom left), and $\Gamma = 6.4$ (bottom right).

separated Gulf Stream is evident at the boundary of the subtropical and subpolar gyre.

In both experiments, outcropping in the northern part is limited to the interior of the subpolar gyre, indicating a weak thermal driving. In the hybrid model of *Huang* [1989], outcropping of the third isopycnal layer was shown as a function of Γ. Due to the strong wind forcing and the shallow depth of the upper two layers, the third layer always outcropped. For $\Gamma < 1.2$, outcropping of the third layer occurred within the subpolar gyre; for $\Gamma > 3.6$ the outcropping zone was adjacent to the northern boundary.

The subtropical gyre is clearly visible in the upper layer thickness fields, demonstrating the dominance of wind forcing over buoyancy forcing in this calculation. The instantaneous upper layer thickness field for experiment 2 shows a highly turbulent flow, with a much narrower and more

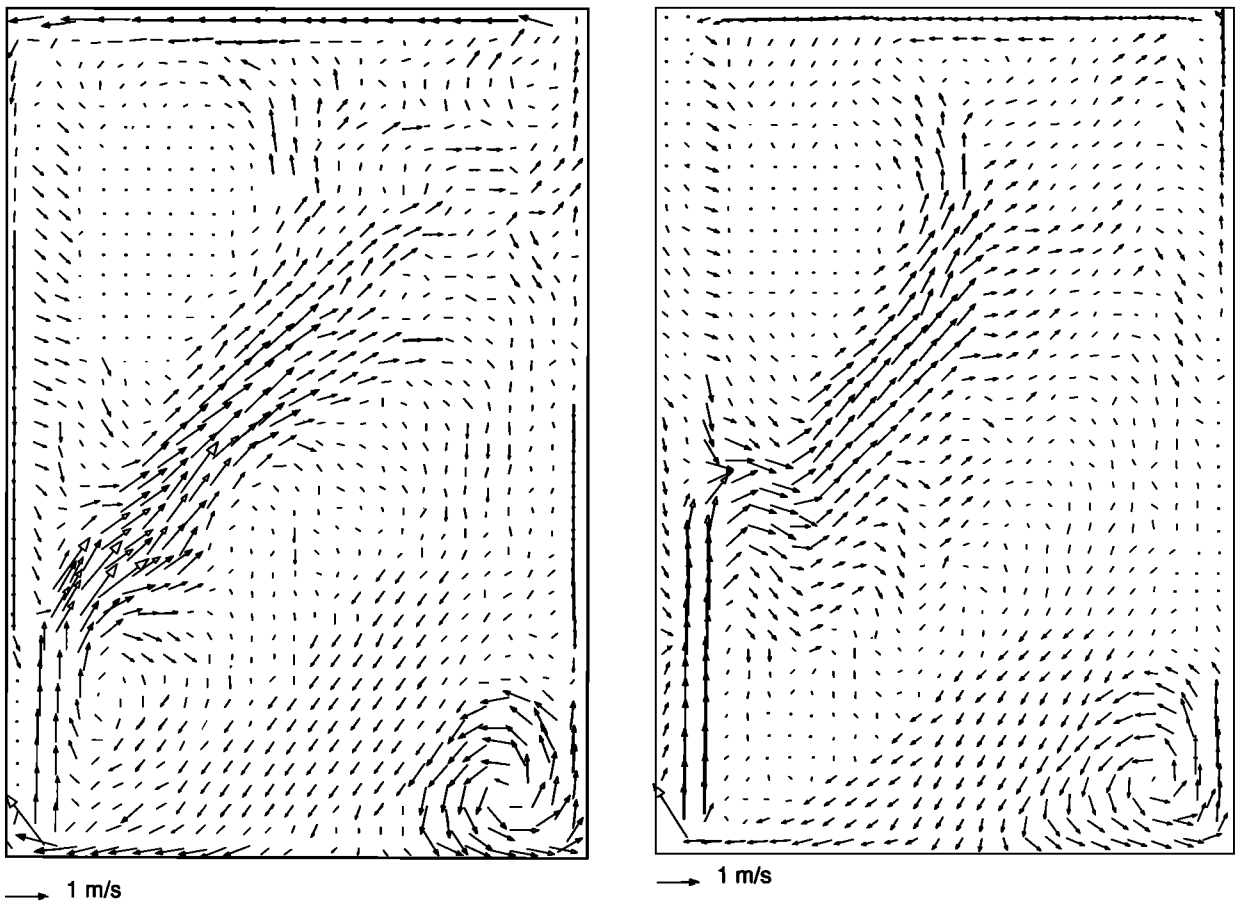

Figure 4. Time-averaged upper layer velocity fields for experiment 2 for (left) $\Gamma = 0.4$ and (right) $\Gamma = 3.2$.

intense Gulf Stream, strongly meandering. The basin is filled with numerous eddies. The birth of a cold core ring is an outstanding feature in this figure.

As might be expected, varying the thermal driving affects the upper layer circulation markedly (Figure 3). It is seen that for $\Gamma = 1.6$ the outcropping area has moved toward the western boundary, blocking the subpolar gyre in the upper layer. The feature of the subtropical gyre is blended by a tendency to form zonal bands of uniform layer depth as a local response to the thermal forcing. For $\Gamma = 3.2$ and $\Gamma = 6.4$ the thermal forcing dominates the upper layer thickness field, and the signature of the midlatitude jet in this field has almost disappeared.

Increasing Γ destroys the surface signal of the warm water pool of the subtropical gyre (Figure 3). Wind forcing induces downwelling there, but the associated heat advection cannot compensate for the atmospheric heat loss when $\Gamma > 1$. Also the return flow advects colder water into this region as the upper layer velocities do not follow thickness contours anymore (Figures 3 and 4). When $\Gamma > 1$ the western boundary current crosses more thickness contours and advects warmer water northward. The thickness contours are pushed further north along its axis, creating a standing meander near the western boundary. As a result, the latitude at which the midlatitude jet leaves the coast is increased.

Also the southward flowing western boundary current of the subpolar gyre is blocked in the upper layer for the larger Γ experiment, which again influences the position at which the Gulf Stream leaves the coast (see also *Thompson and Schmitz* [1989]).

From Figures 3 and 5 the upper layer thickness fields for solutions with and without eddies, respectively, can be compared for different values for Γ (0.4 and 3.2). It is seen that the eddies significantly enhance the tendency of the air/sea interaction to increase the latitude at which the midlatitude jet leaves the coast. This is accomplished by enhancing the velocity of the western boundary current and the subsequent meander that forms at the turning position. Increasing Γ from 0.4 to 3.2 shifts the position where the midlatitude jet leaves the coast further northward. Enhancing Γ even further has no significant effect. The coupling between the SST field and the atmospheric thermal forcing is then already so strong that an increase of this forcing does not change the upper layer thickness field in the subtropical gyre.

The eddies induce a standing wave in the midlatitude jet (see also *Drijfhout* [1994, section 4]). This standing wave has an anticyclonic meander where the boundary current turns eastward and leaves the coast. Comparing Figures 3, 4, and 5, it can be concluded that the eddies, together with the change in friction parameterization from Laplacian to biharmonic friction, significantly modify the vorticity budget of the western boundary current where it turns eastward, and subsequently the dynamics that govern the separation of the midlatitude jet from the coast. Also the eddies make the model flow field more sensitive to the effect of an enhanced

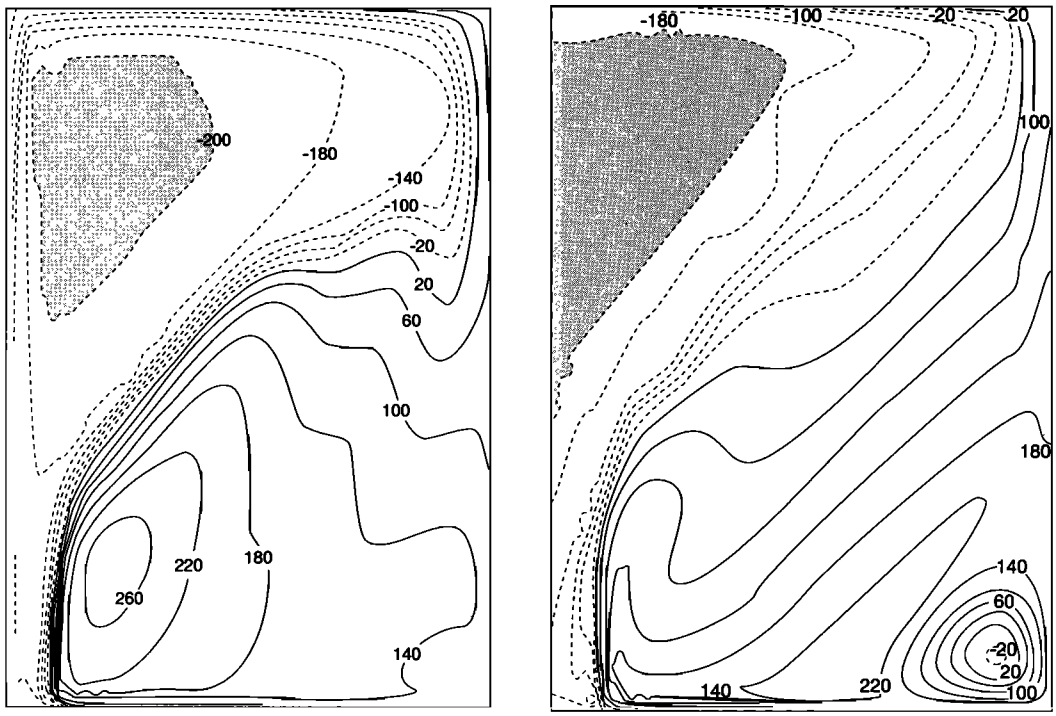

Figure 5. Time-averaged upper layer thickness fields for experiment 1 for (left) $\Gamma = 0.4$ and (right) $\Gamma = 3.2$.

thermal driving. While Γ increases, the upper layer thickness field changes from a wind-forced pattern to a thermally forced pattern. This feature is blended by a northward deflection of isopycnals in the western boundary current, controlled by the strength of the advection. The latter is significantly increased by the eddies.

4. Meridional Heat Transport

The meridional (poleward) heat transport can be evaluated by integrating the zonally and vertically integrated form of the heat budget equation:

$$\frac{\partial}{\partial t} T + \nabla \cdot (\mathbf{u}T) = -B_T \nabla^4 T + \gamma(T^* - T) \qquad (4')$$

from the southern boundary to a latitude y_0.

We then obtain, from the thickness advection, the poleward heat transport at latitude y_0, balanced by the integrals of the surface flux, diffusion, and tendency (heat storage).

This balance is illustrated for experiments 1 and 2 with $\Gamma = 0.4$ (Figure 6). The meridional heat transport in this model is composed of the transport by the wind-scale overturning cells, northward in the subtropics, southward in midlatitudes; the northward heat transport by the subtropical and subpolar gyres; and the eddy heat transport. This results in a minimum in heat transport at the position of the central jet. (Deep convection which could produce a basin-scale overturning was excluded as a mode of heat transport.)

The integrated surface heat flux is very similar for the two experiments: The eddies do not significantly change the zonally averaged upper layer temperature field if the thermal driving is weak. A negligible net heat transport by the eddies can even occur when the eddy heat transport itself is a first-order quantity (Figure 7). There is a large northward heat transport by the eddies at the latitude of the central jet, which is the primary source of baroclinic instability in the model. When the thermal driving is weak, the eddy heat transport and the eddy-induced change in heat transport by the mean flow nearly compensate. A (tentative) explanation for this feature has been given by *Drijfhout* [1994, section 5].

Six twin experiments, with and without eddies, have been performed for different values of Γ (Table 1). In all the runs the eddy heat transport remains of the same order of magnitude (Figure 8). The maximum in the central jet region decreases and broadens somewhat for larger Γ. As the gradient in air temperature is smaller than the temperature front between the subpolar and subtropical gyre, an enhanced thermal driving smears out the upper layer temperature gradient in this region (Figure 3). As a consequence the central jet becomes somewhat less unstable. The southward heat transport at 23°N is related to the boundary jet between the subtropical gyre and the anticyclone in the southern corner. This jet shows a weak baroclinic instability. In reality, baroclinic instability is likely to be important in the North Equatorial Current. The representation in the present geometry, however, does not warrant detailed investigation. We will not comment further on this feature as it does not pertain to the questions at hand.

The eddy-induced change in total heat transport strongly increases between $\Gamma = 0.8$ and $\Gamma = 3.2$ (Figure 8). From $\Gamma = 3.2$ to $\Gamma = 12.8$ it remains nearly constant, of the same order of magnitude as the eddy heat transport itself. This is consistent with the behavior of the upper layer thickness

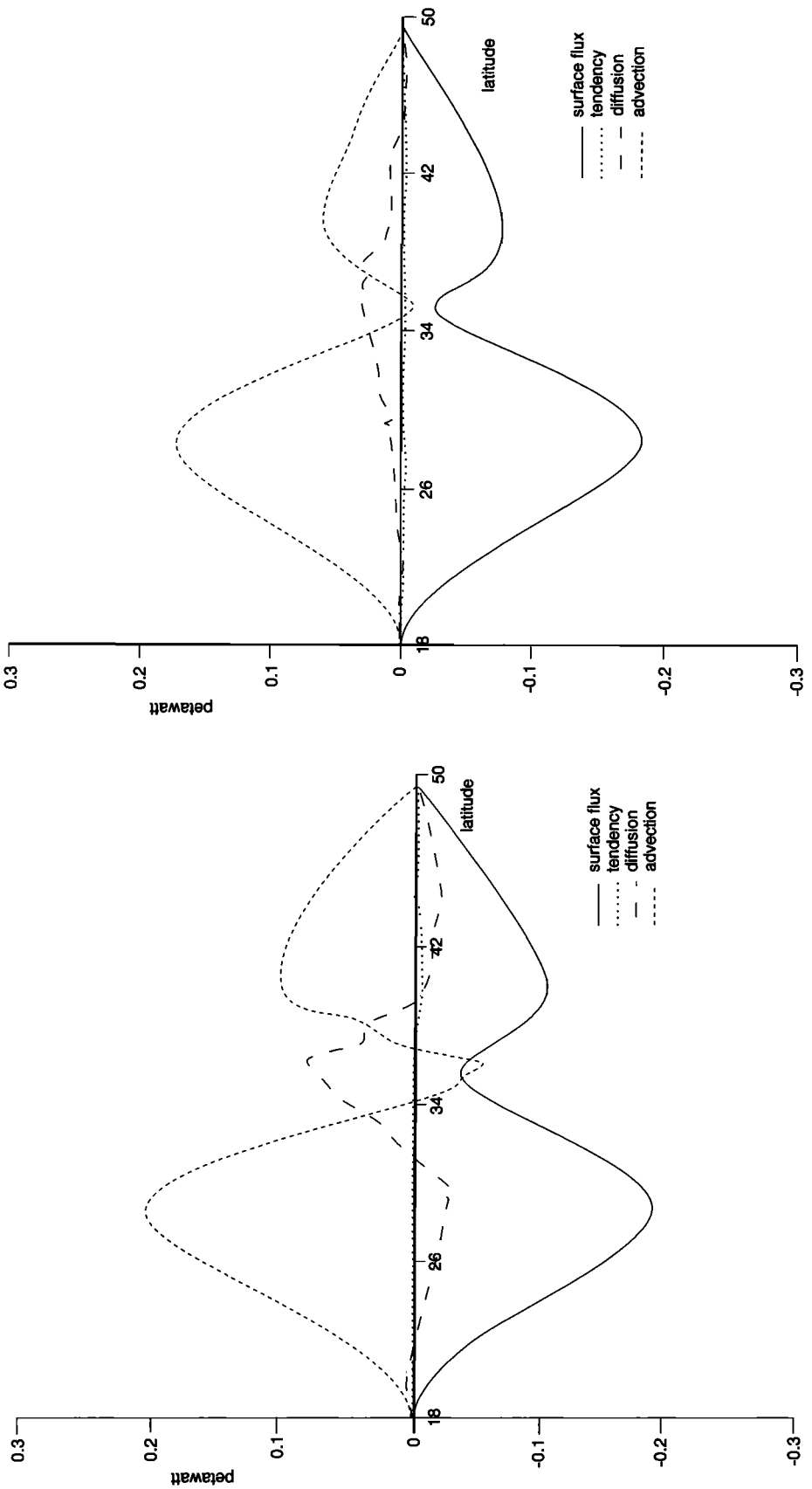

Figure 6. Heat transport in petawatts for (left) experiment 1 and (right) experiment 2 for $\Gamma = 0.4$. Shown are the integrated forms of heat advection, diffusion, surface flux, and tendency.

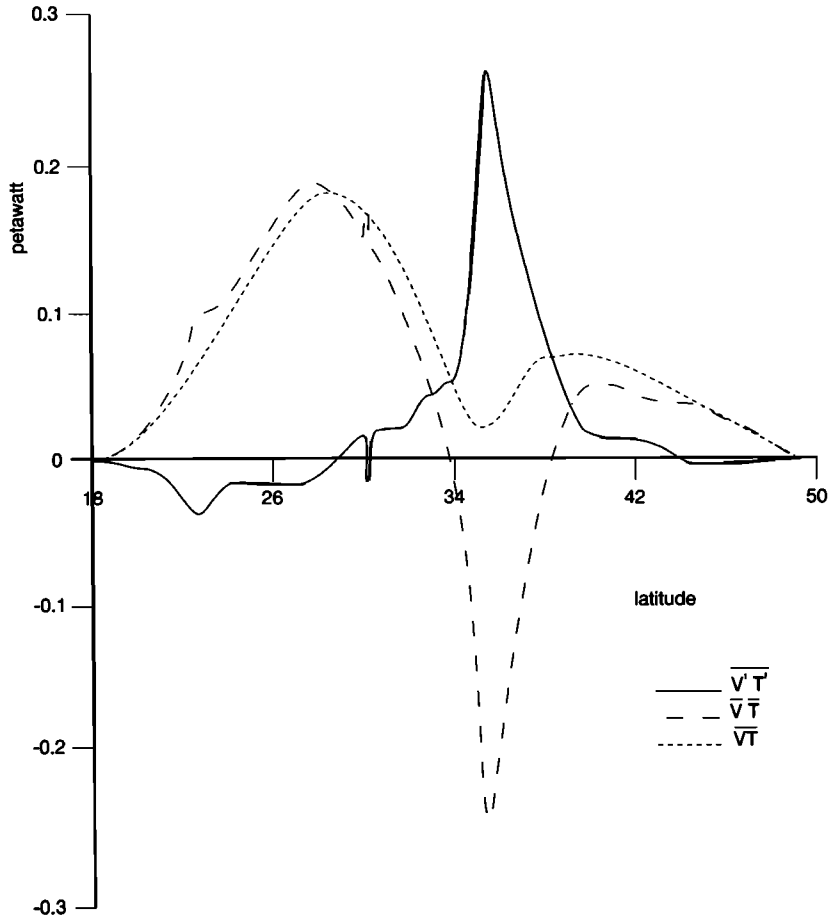

Figure 7. Heat transport for experiment 2 ($\Gamma = 0.4$). Shown are the total heat transport (advection plus diffusion), the eddy heat transport, and the heat transport by the mean flow.

field, which also does not change by increasing Γ to values larger than 3.2.

It can be concluded that in this model, with respect to eddy–mean flow interaction, the thermal driving changes from weak to strong between $\Gamma = 1$ and $\Gamma = 3$. This means that the intermediate range lies between 150 and 50 days for the SST relaxation time. The strength of the thermal driving, however, is not determined by the restoring time only, but by the product of restoring time and upper layer depth. So the restoring times for which transition from "weak" to "strong" occur depend on the upper layer depth of the model. A better parameter to denote the strength of the coupling is the thermal coupling coefficient. A transition occurs for coupling coefficients between 70 W m^{-2} K^{-1} and 200 W m^{-2} K^{-1}. *Bretherton* [1982] suggests that the thermal coupling coefficient for small-scale SST anomalies should be about 100 W m^{-2} K^{-1}. In that case, the thermal coupling for eddies falls within the transition regime. Moreover, in the present model the thermal coupling coefficients which denote the transition regime are probably on the high side. Γ controls the coupling, and τ will be on the high side as the wind-driven velocity U is rather large in the present model, due to the specific geometry and the wind forcing used.

The values for Γ that denote transition suggest that the model of *Cox* [1985] and followers is in the regime of weak thermal driving. Although the SST relaxation time is only 50 days in the Cox model, the upper layer depth is 35 m, and the thermal coupling coefficient is about 35 W m^{-2} K^{-1}. However, due to the rather crude representation of mixed layer processes in this and other ocean general circulation models (GCMs), it is difficult to draw quantitative conclusions. It can only be concluded that transition from weak to strong thermal driving occurs for realistic values of the SST relaxation time. In the next section we will comment on the mechanism by which the coupling influences the eddy–mean flow interaction and the eddy-induced change in heat transport.

5. Eddy-Mean Flow Interaction

5.1. Overturning Anomalies

Compensation of the eddy heat transport was found by *Cox* [1985], *Böning and Budich* [1992], and *Drijfhout* [1994]. *Bryan* [1991] suggested that this compensation consisted of an enhancement of the wind-scale overturning cells, which compensates the heat transport driven by baroclinic instability. The enhancement of the southward heat transport by the wind-scale overturning at midlatitudes is demonstrated in Figure 9 for $\Gamma = 0.4$. This extra southward heat transport compensates the northward eddy heat transport there.

When Γ is increased to 3.2, the eddy-induced overturning anomaly becomes more complicated (Figure 10). The anticlockwise meridional overturning cell at midlatitudes has intensified, but it is displaced downward in the vertical. On

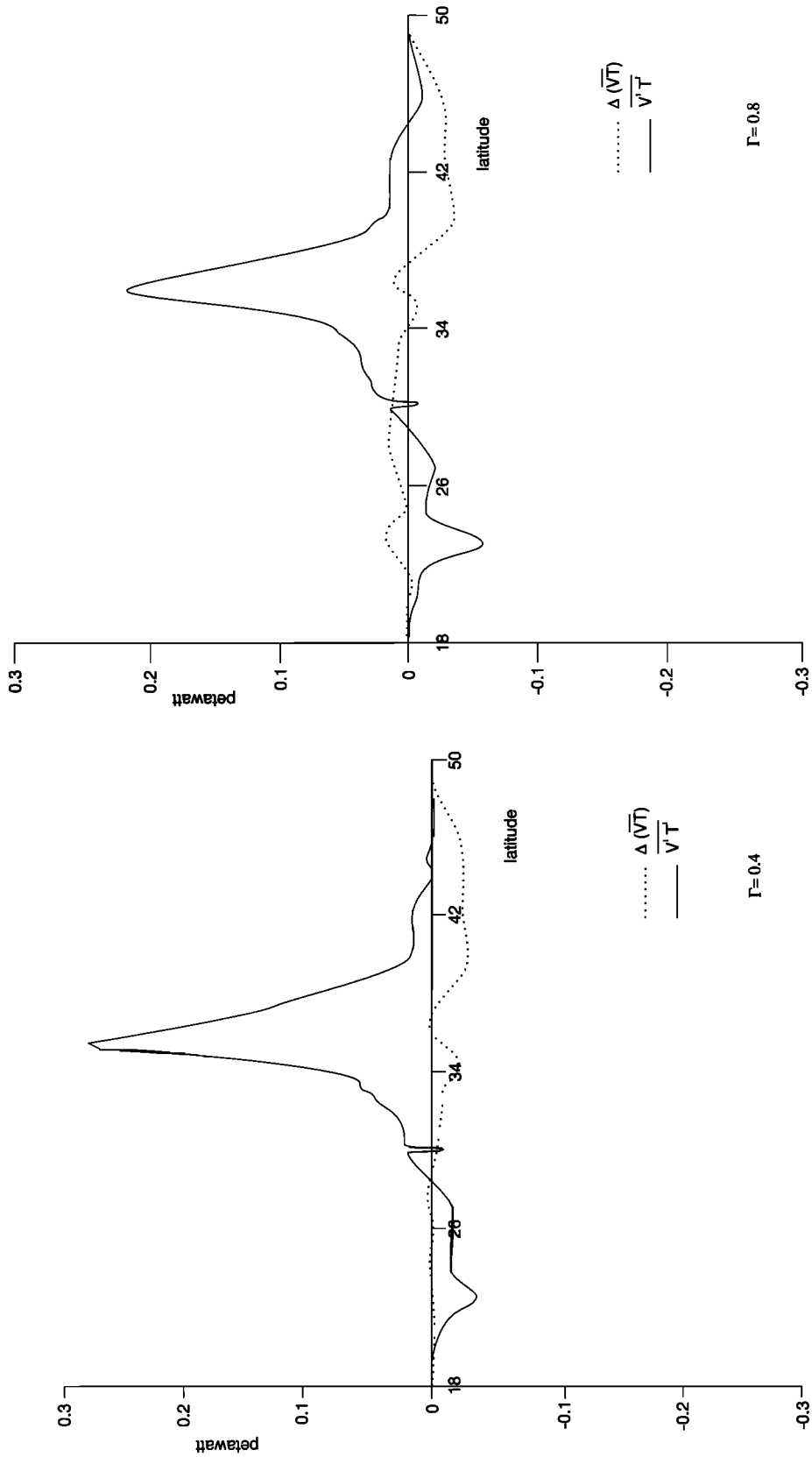

Figure 8. Heat transport for six runs, varying Γ from 0.4 to 12.8. Shown are the eddy heat transport and the eddy-induced change in total heat transport.

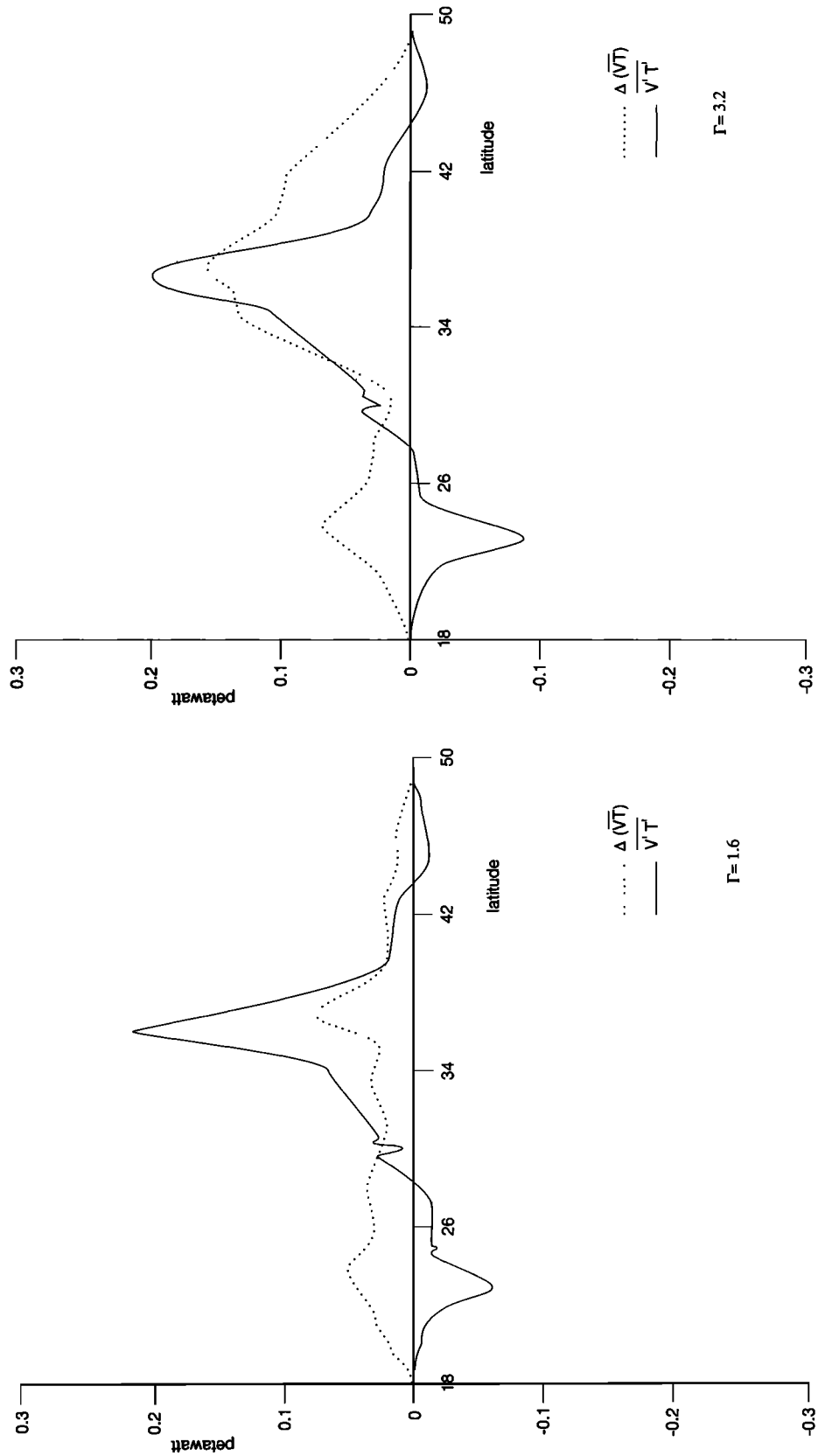

Figure 8. (continued)

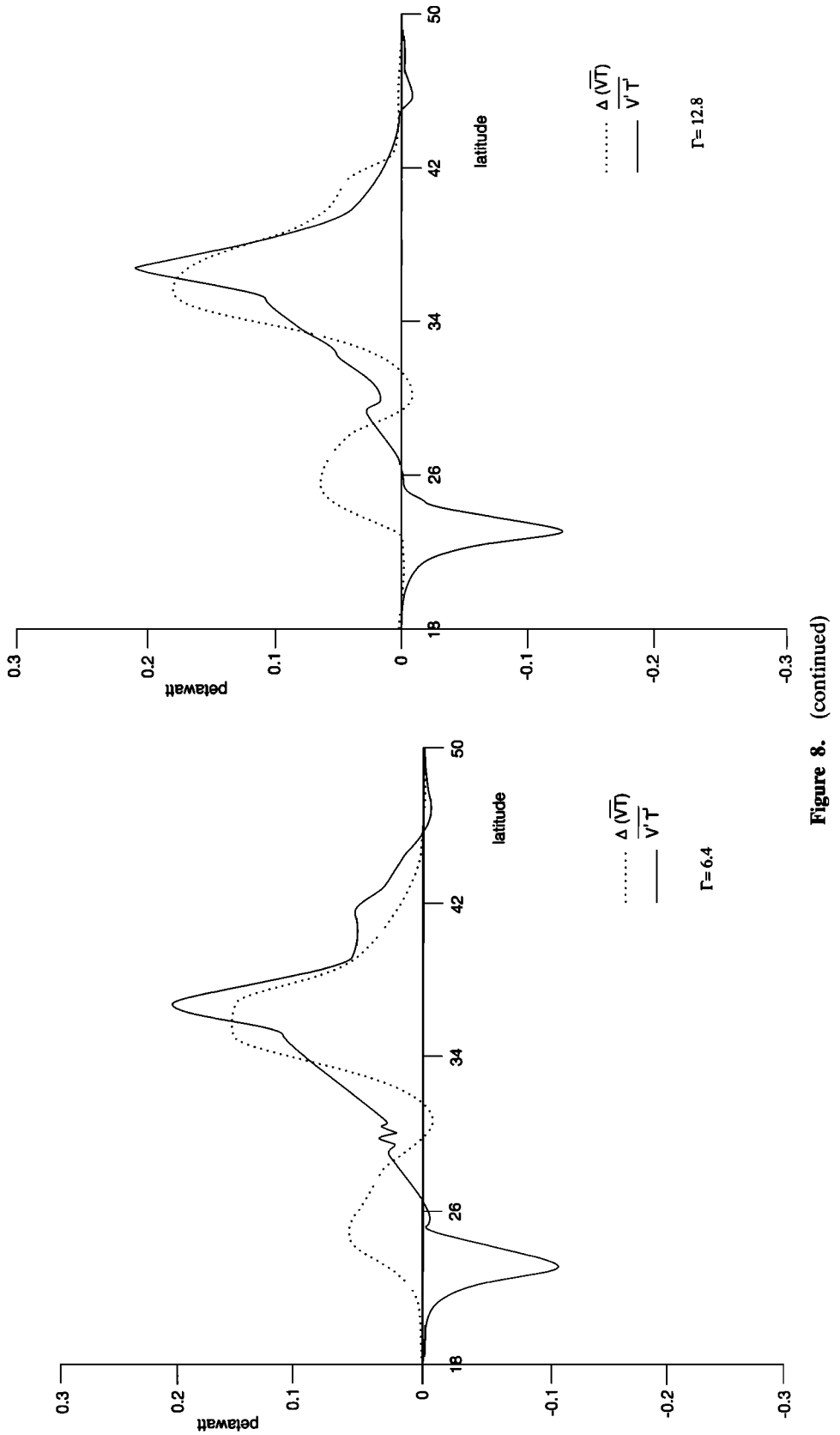

Figure 8. (continued)

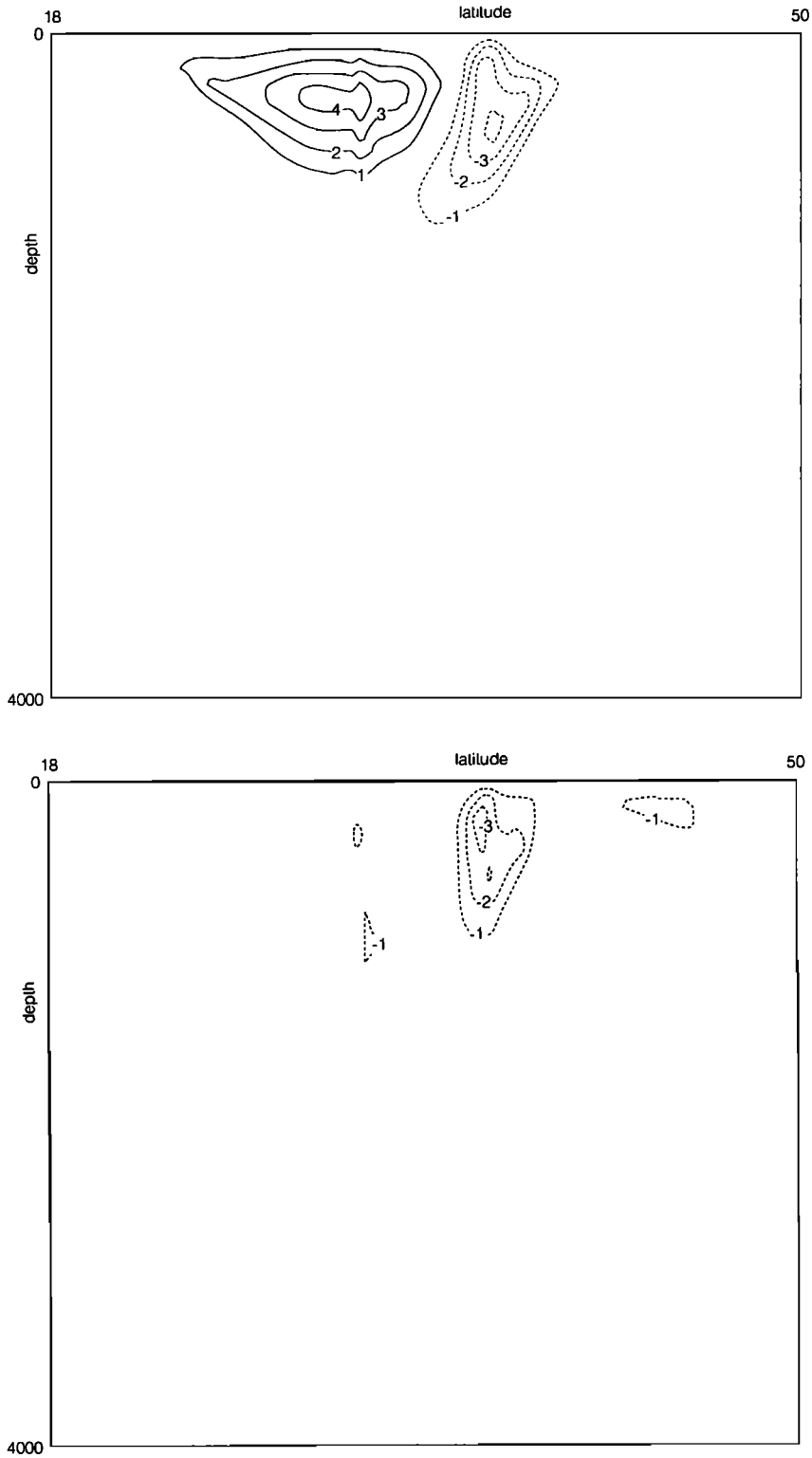

Figure 9. (top) Meridional transport function for experiment 2 and (bottom) the difference in meridional transport function between experiments 2 and 1, for $\Gamma = 0.4$. Values are in sverdrups.

top of it there has appeared a clockwise overturning cell that is connected with the subpolar wind-scale overturning. These two eddy-induced overturning anomalies nearly compensate at midlatitudes, so the eddy heat transport in this region can no longer be balanced by an eddy-induced change in mean heat transport.

Bryan [1986] has pointed out that modification of the wind-scale overturning cells should be associated with a change in the cross-basin zonal pressure gradient. In the upper layer the change in cross-basin zonal pressure gradient and meridional flow have reversed between $\Gamma = 0.4$ and $\Gamma = 3.2$ (Figure 11). This is consistent with the eddy-induced

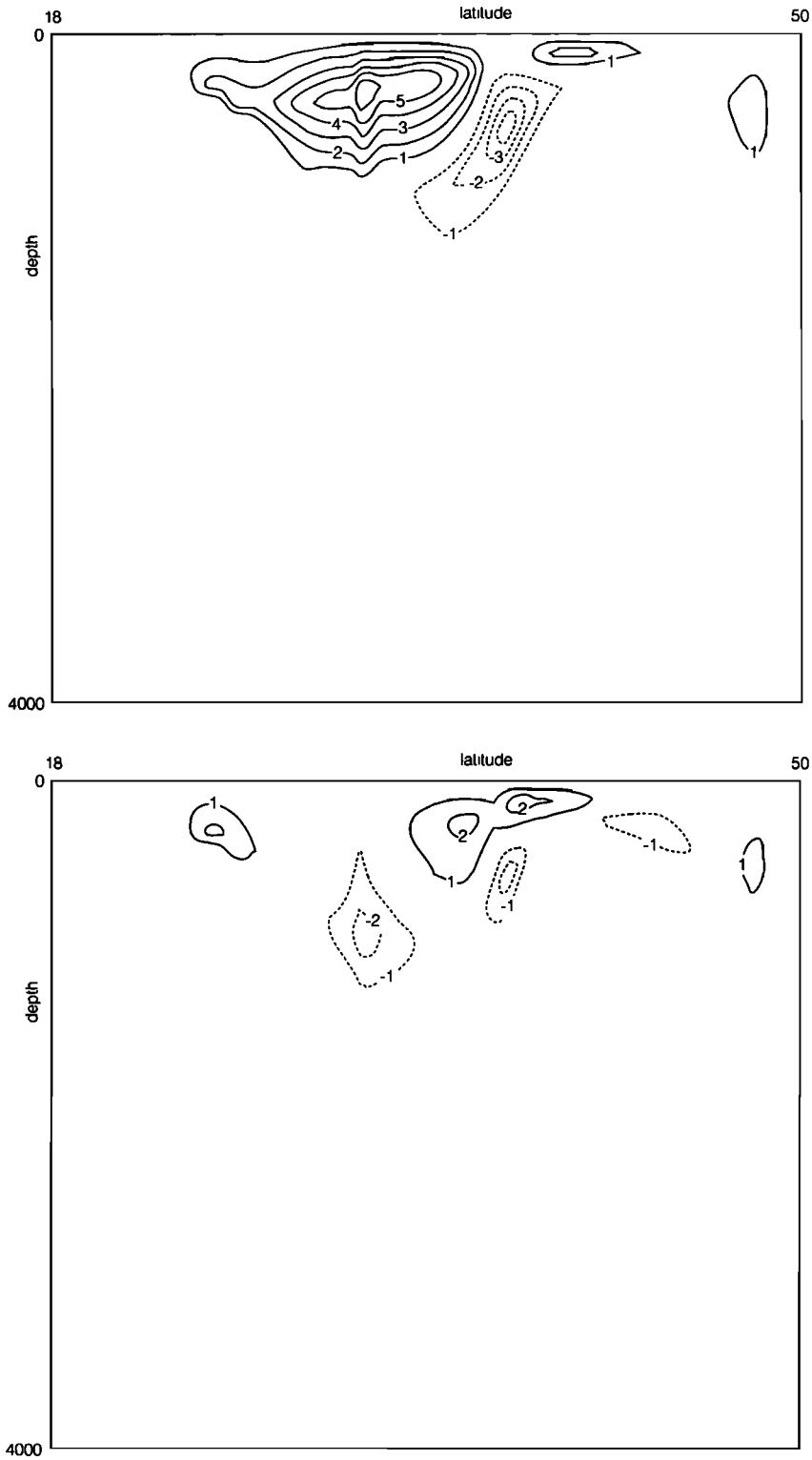

Figure 10. (top) Meridional transport function for experiment 2 and (bottom) the difference in meridional transport function between experiments 2 and 1, for $\Gamma = 3.2$.

change in overturning (Figures 9 and 10). (The overturning anomalies show a better geostrophic balance than that from *Drijfhout* [1994], because experiment 2 in that study was performed with a higher resolution and lower dissipation, with consequently larger Rossby number.)

To elucidate the cause for a reversal of the eddy-induced change in cross-basin pressure gradient when Γ is increased from 0.4 to 3.2, the difference in upper layer thickness between experiments 1 and 2 for $\Gamma = 0.4$ and 3.2 is shown (Figure 12). For $\Gamma = 0.4$ the western side of the basin has become warmer at midlatitudes, the eastern side cooler (see also *Drijfhout* [1994]). When Γ increases, the stream function

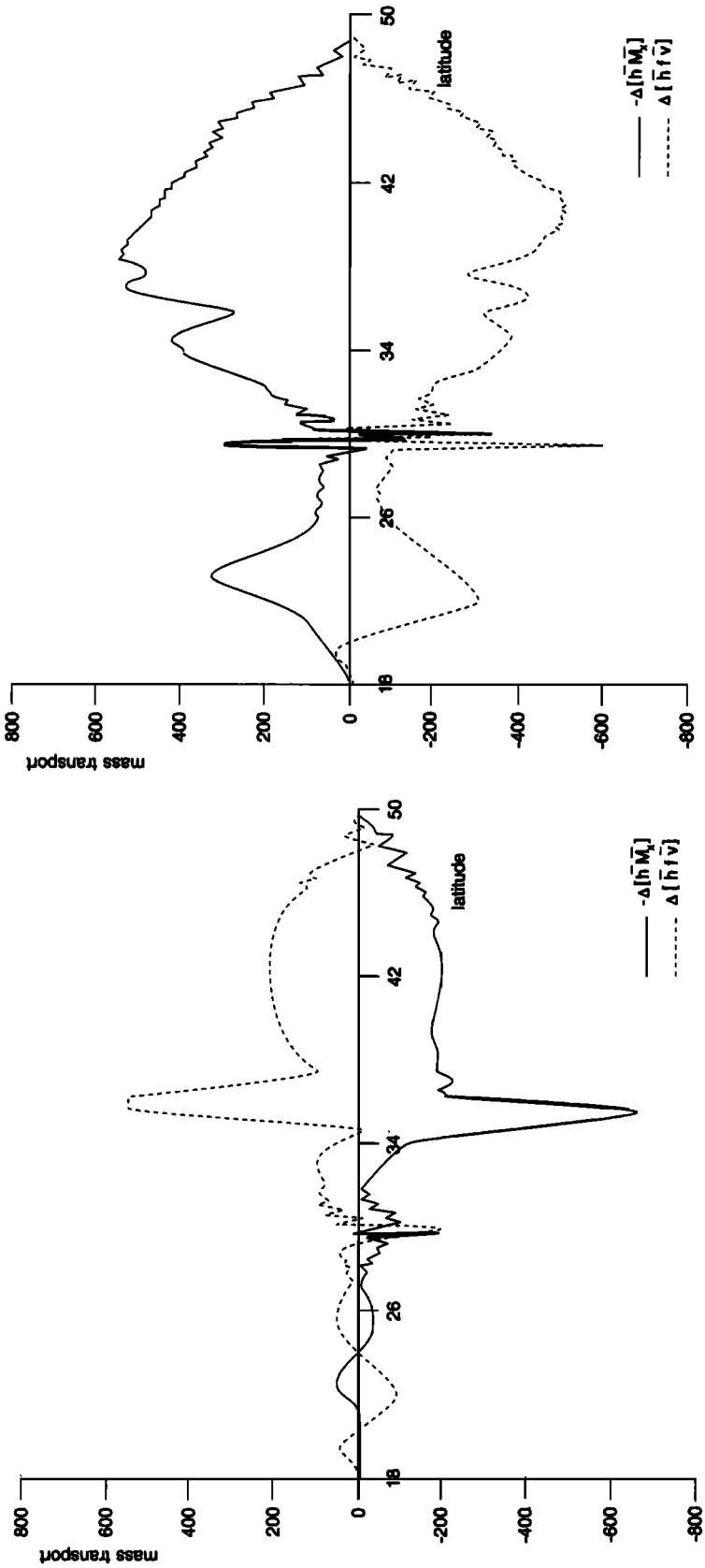

Figure 11. The eddy-induced change in the zonally integrated upper layer zonal momentum balance, for (left) $\Gamma = 0.4$ and (right) $\Gamma = 3.2$. (Terms are multiplied with the layer depth.) Shown are $f\Delta[\bar{h}\bar{v}]$ and $-\Delta[\bar{h}\bar{M}_x]$. Values are in $m^3\ s^{-2}$.

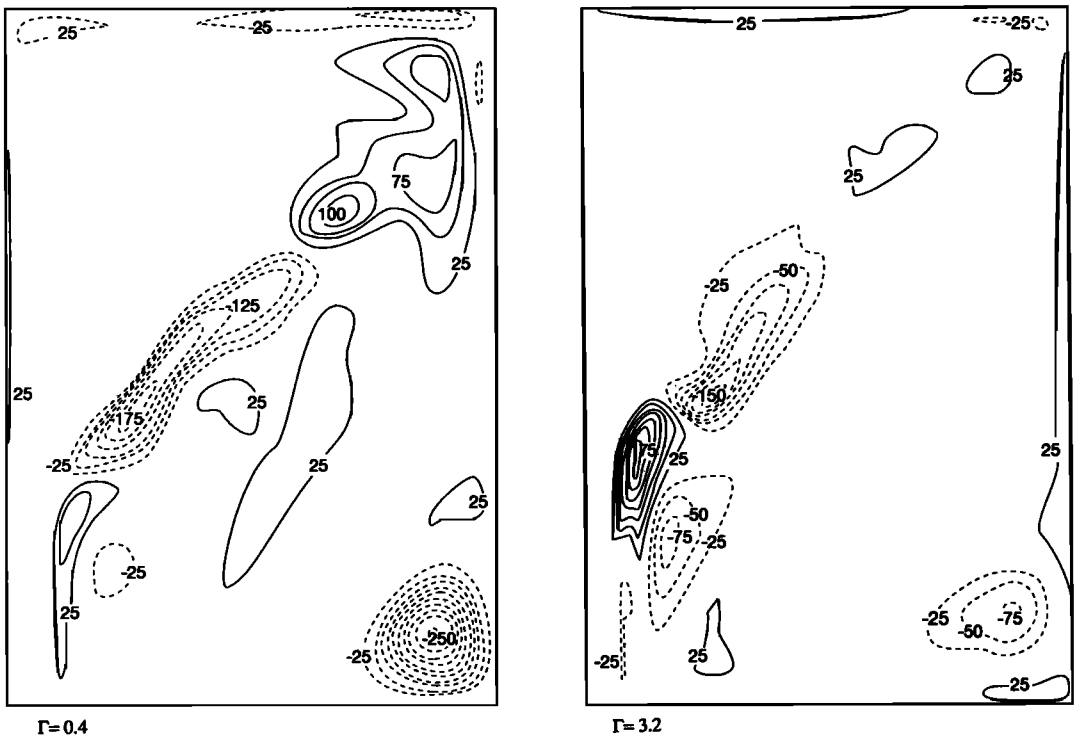

Figure 12. The difference in upper layer thickness between experiments 1 and 2, for (left) $\Gamma = 0.4$ and (right) $\Gamma = 3.2$.

maximum related to the subtropical gyre has split into two, indicating the establishment of a tight recirculation zone southwest of the midlatitude jet (Figure 13). The physical mechanism which is responsible for establishing this recirculation is not completely clear. In eddy-resolving, wind-driven studies such a recirculation has also been found [e.g., *Holland*, 1978]; in that case, Reynolds stresses during the transfer from eddy to mean kinetic energy are responsible

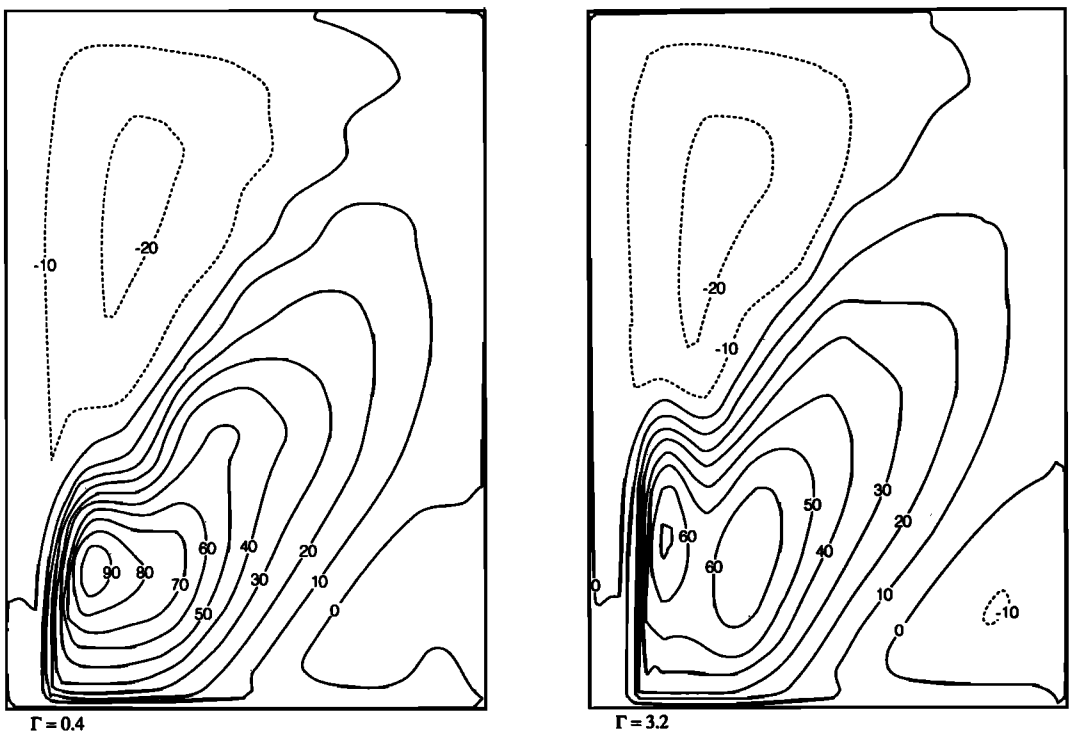

Figure 13. Time-averaged barotropic stream function for experiment 2, for (left) $\Gamma = 0.4$ and (right) $\Gamma = 3.2$.

for establishing this circulation. Also in non-eddy-resolving models such a recirculation has been demonstrated to result from cooling the subtropical gyre [e.g., *Colin de Verdière*, 1989; *Huang*, 1990]. In the present study both the eddies and increased cooling enhance the recirculation.

The effect of this recirculation is to bring warm water from the western boundary current further to the northeast; the latitude at which the midlatitude jet separates from the coast is increased by this recirculation (Figures 3, 4, and 5). As this water is warmer than the air, it is cooled on its path. The southwest branch of the recirculation brings relatively cold water back in the western boundary current (Figures 12 and 13). By this mechanism the eddies cool the western boundary, while in the absence of such a tight recirculation the western boundary at midlatitudes is warmed.

5.2. The Role of Diabatic Forcing

The critical role of the diabatic forcing in the explanation of the compensation of the eddy heat transport was first mentioned by *Bryan* [1986]. He argued that the ocean was subjected to weak thermal driving and for that reason there should be similarities between the compensation of the eddy heat transport in the ocean and heat transport by stratospheric waves [e.g., *Andrews et al.*, 1987]. This suggests the existence of a nonacceleration theorem and the applicability of a generalized Eliassen-Palm approach [e.g., *Eliassen and Palm*, 1961; *Andrews and McIntyre*, 1976] to explain the eddy heat transport compensation in the ocean.

However, to apply such a theory to the transient eddies implies the development of an equivalent of the Eliassen-Palm concept in time-averaged conditions. This is far from trivial. Also the concept of a steady wave field, central in the Andrews and McIntyre theory, seems inapplicable to the simulations of ring formation (e.g., *Drijfhout* [1990]; see *Drijfhout* [1994] for a more complete discussion). In the latter study an eddy–mean flow interaction theorem in isopycnic coordinates was derived for weak thermal driving:

$$\Delta[\Lambda] = \bar{h}\Delta[\bar{M}_x] \tag{6}$$

where Λ is the mean flow forcing by the eddies:

$$\Lambda = \{\overline{(hv)'u'}\}_y + \{\overline{h'M'_x}\} \tag{7}$$

and $\bar{x}$ is defined as the zonal average of x, $[x]$ as the time average, and $x' = x - \bar{x}$. (For the meaning of h, u, v, and M see equations (1)–(4).)

The meaning of Δ in (6) is defined as follows: Consider an experiment without transient eddies, experiment 1, and an experiment with transient eddies, experiment 2. Then $\Delta[\bar{x}]$ denotes $[\bar{x}]^2 - [\bar{x}]^1$, i.e., the eddy-induced change in the mean flow quantity $[\bar{x}]$.

Equation (6) states that the eddy-induced change in zonal pressure gradient is forced by the transient eddy contribution to the mean flow forcing. This eddy–mean flow interaction secures the net non–heat transport character of the transient eddies. A more general form of (6) is

$$f\Delta[\bar{V}] + \Delta[\Lambda + \bar{X} - \bar{h}\bar{M}_X] = 0 \tag{8}$$

where X is any nonconservative force. When the thermal driving is weak it can be argued [*Drijfhout*, 1994] that $f\Delta[\bar{V}]$ and $\Delta[\bar{X}]$ are small and (6) applies. If the thermal driving is not weak, (8) should be considered.

Equation (6) is a good approximation for the case $\Gamma = 0.4$, while for $\Gamma = 3.2$ it is not (Figure 14). When the coupling is strong, i.e., $\Gamma > 3$ in this model, the eddy–mean flow interaction principle expressed by (6) breaks down, and consequently the non–heat transport character of the eddies.

The role of diabatic forcing in this eddy–mean flow interaction is controlled by the nondimensional parameter Γ, which measures the ratio of the timescales of the wind driven circulation to the SST relaxation. The influence of thermal forcing increases significantly between $\Gamma = 1$ and 3, i.e., SST relaxation times of 150 and 50 days, or thermal coupling coefficients of 70 and 200 W m^{-2} K^{-1} for the present model.

6. Summary and Conclusions

In the present study it was investigated how the diabatic forcing influences the eddy–mean flow interaction. The experiments were carried out with an isopycnic model, derived from the code of *Bleck and Boudra* [1986], that simulates the idealized North Atlantic gyre study of *Semtner and Mintz* [1977]. When varying the SST relaxation timescale for each run, two experiments were made, one experiment with high Laplacian dissipation which suppresses all transient behavior, and one with weak biharmonic dissipation in which the subsequent hydrodynamic instability of the flow gives rise to a vigorous eddy field.

An increase of the nondimensional air/sea interaction coefficient induces an increase of the angle between the upper layer velocities and thickness contours, and also the absolute velocity itself is increased. The latter feature is enhanced by the eddies. Then, in the boundary current where the velocity is largest, the thickness contours are pushed further northward, which creates a standing meander near the western boundary. As a result the latitude at which the midlatitude jet leaves the coast is increased.

A tight recirculation just southwest of the midlatitude jet is established for sufficiently large Γ. This circulation is enhanced by the eddies. For $\Gamma > 3$ the cold water advection by the recirculation gyre cools the western boundary. For $\Gamma < 1$ the eddy-induced increase of warm water advection by the western boundary current is the dominating temperature effect. The range $1 < \Gamma < 3$ is a transition regime.

The subsequent change in cross-basin zonal pressure gradient induces overturning anomalies. For weak thermal driving the eddy-induced overturning anomalies compensate the eddy heat transport. For strong thermal driving the eddy-induced change in the upper layer zonal pressure gradient reverses. The eddy-induced change in total heat transport becomes of the same order as the eddy heat transport itself.

Bryan [1986] argued that the weak thermal driving of the ocean necessitates the compensation of the eddy heat transport. *Drijfhout* [1994] extended the discussion on the critical role of diabatic effects by including a nondimensional parameter Γ which measures the ratio of the advective timescale and the SST relaxation. In the present study it has been shown that Γ controls the eddy–mean flow interaction. For two different definitions of the relevant advective length scale, the transition between weak and strong driving occurs between $1 < \Gamma < 3$ or $0.3 < \Gamma < 1$, respectively. This implies that from the present study it cannot be concluded whether the timescale of mesoscale eddies is determined by the advective timescale of the wind-driven flow, i.e., the time

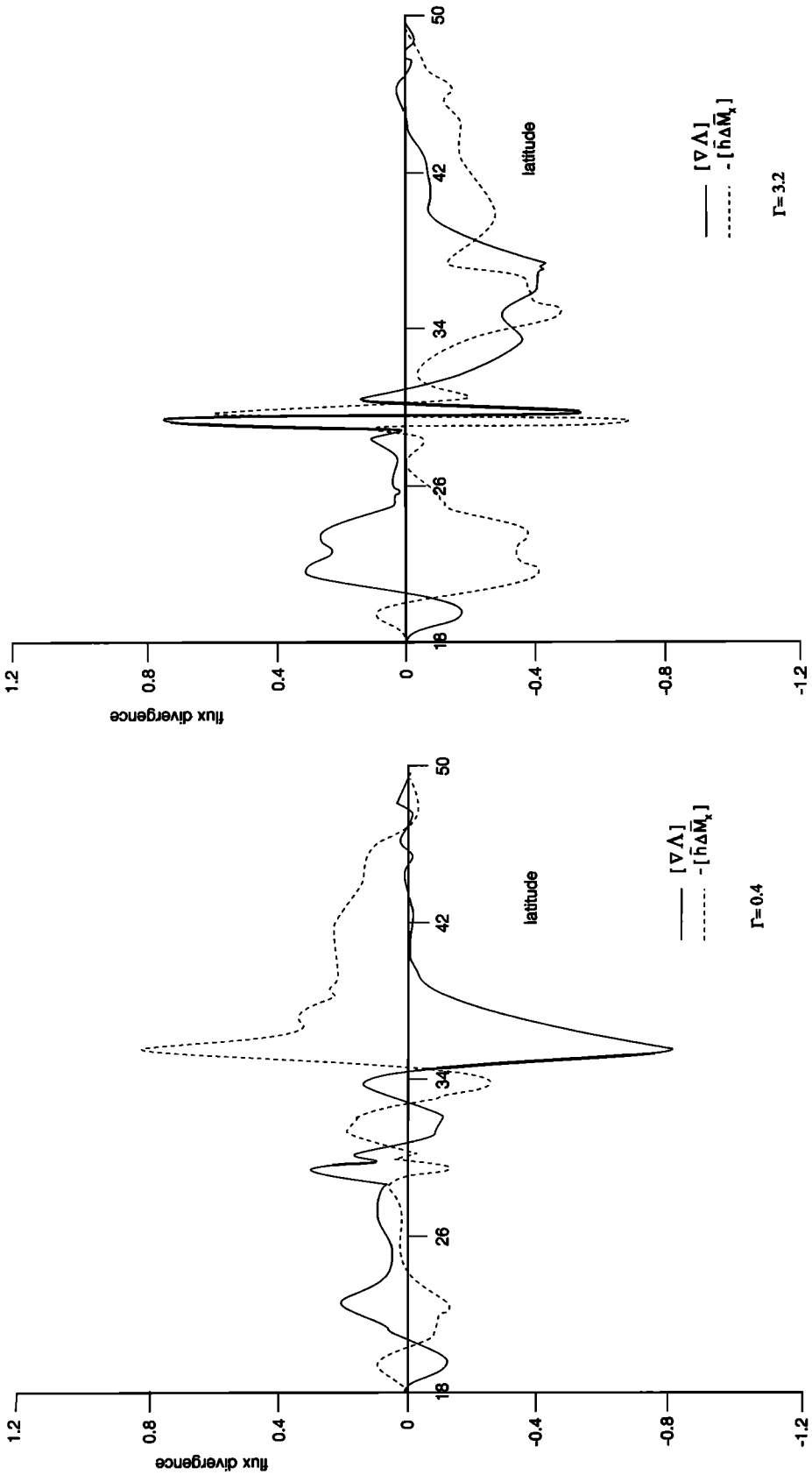

Figure 14. The transient eddy-induced change in the mean flow forcing $\Delta[\Lambda]$ and $-[\bar{h}\Delta\bar{M}_x]$, for (left) $\Gamma = 0.4$ and (right) $\Gamma = 3.2$. Values are in 10^{-2} m^2 s^{-2}.

needed to bring an isolated eddy back into the western boundary current, or the advection timescale of the SST anomaly by the background flow and phase velocity of the eddy.

It was shown that for weak thermal driving the contribution of the transient eddies to the mean flow forcing is almost balanced by an eddy-induced change in cross-basin zonal pressure gradient. For intermediate and strong thermal driving this eddy–mean flow interaction breaks down. As a result, the eddy–mean flow interaction changes drastically in the range $1 < \Gamma < 3$ (i.e., SST relaxation times between 150 and 50 days, or thermal coupling coefficients of 70 and 200 W m^{-2} K^{-1}), showing a complete breakdown of the eddy heat transport compensation. This transition regime, however, will depend on the parameterization of air/sea interaction, the mixed layer physics, and the effective depth of the mixed layer in the model. In the present model the mixed layer is a purely isopycnal layer with an average depth of 200 m. In general, the relaxation time for transition will roughly be proportional to the effective depth of the model mixed layer.

The results of this study have been obtained with a rather simple model and a crude parameterization of the air/sea interaction. No quantitative conclusions can be drawn from this study. Its main results are that the eddy heat transport compensation is not a general model feature; it depends on the air/sea interaction, and it possibly can break down for realistic values of this coupling. However, both observations and more complete models are needed to infer the strength of the real air/sea coupling and the role of eddies in the ocean heat budget.

Acknowledgments. This research was supported by the European Economic Community (EEC). Arie Kattenberg is acknowledged gratefully for comments on an earlier version on this manuscript and discussion from which this study benefited. Also the helpful comments of an anonymous referee are appreciated.

References

Andrews, D. G., and M. E. McIntyre, Planetary waves in horizontal and vertical shear: The generalized Eliassen-Palm relation and the mean zonal acceleration, *J. Atmos. Sci.*, *33*, 2031–2048, 1976.

Andrews, D. G., J. R. Holton, and C. B. Leovy, *Middle Atmospheric Dynamics*, 489 pp., Academic, San Diego, Calif., 1987.

Bleck, R., and D. B. Boudra, Wind driven spin-up in eddy-resolving ocean models formulated in isopycnic and isobaric coordinates, *J. Geophys. Res.*, *91*, 7611–7621, 1986.

Böning, C. W., and R. C. Budich, Eddy dynamics in a primitive equation model: Sensitivity to horizontal resolution and friction, *J. Phys. Oceanogr.*, *22*, 361–381, 1992.

Bretherton, F. P., Ocean climate modeling, *Prog. Oceanogr.*, *11*, 93–129, 1982.

Bryan, K., Poleward buoyancy transport in the ocean and mesoscale eddies, *J. Phys. Oceanogr.*, *16*, 927–933, 1986.

Bryan, K., Poleward heat transport in the ocean, *Tellus*, *43*, 104–115, 1991.

Colin de Verdière, A., On the interaction of wind and buoyancy driven gyres, *J. Mar. Res.*, *47*, 595–633, 1989.

Cox, M. D., An eddy-resolving numerical model of the ventilated thermocline, *J. Phys. Oceanogr.*, *15*, 1312–1324, 1985.

Cox, M. D., and K. Bryan, A numerical model of the ventilated thermocline, *J. Phys. Oceanogr.*, *14*, 674–687, 1984.

Cushman-Roisin, B., On the role of heat flux in the Gulf Stream–Sargasso Sea subtropical gyre system, *J. Phys. Oceanogr.*, *17*, 2189–2202, 1987.

Drijfhout, S. S., Ring genesis and the related transports of heat, momentum and vorticity: A parameter study, *J. Phys. Oceanogr.*, *20*, 1645–1665, 1990.

Drijfhout, S. S., Ring genesis and the related heat transport, II, A model comparison, *J. Phys. Oceanogr.*, *22*, 268–285, 1992.

Drijfhout, S. S., On the heat transport by mesoscale eddies in an ocean circulation model, *J. Phys. Oceanogr.*, *24*, 353–369, 1994.

Eliassen, A., and E. Palm, On the transfer of energy in stationary mountain waves, *Geophys. Norv.*, *22*(3), 1–23, 1961.

Haney, R. L., Surface thermal boundary condition for ocean circulation models, *J. Phys. Oceanogr.*, *1*, 241–248, 1971.

Holland, W. R., The role of mesoscale eddies in the general circulation of the ocean—Numerical experiments using a wind-driven quasi-geostrophic model, *J. Phys. Oceanogr.*, *8*, 363–392, 1978.

Huang, R. X., Sensitivity of a multilayered oceanic general circulation model to the sea surface thermal boundary condition, *J. Geophys. Res.*, *94*, 18,011–18,021, 1989.

Huang, R. X., Does atmospheric cooling drive the Gulf Stream recirculation? *J. Phys. Oceanogr.*, *20*, 750–757, 1990.

Huang, R. X., and K. Bryan, A multilayer model of the thermohaline and wind-driven ocean circulation, *J. Phys. Oceanogr.*, *17*, 1909–1924, 1987.

Luyten, J. R., and H. Stommel, Gyres driven by combined wind and buoyancy flux, *J. Phys. Oceanogr.*, *16*, 1551–1560, 1986.

Luyten, J. R., J. Pedlosky, and H. Stommel, The ventilated thermocline, *J. Phys. Oceanogr.*, *13*, 292–309, 1983.

Pedlosky, J., W. Smith, and J. R. Luyten, On the dynamics of the coupled mixed layer–thermocline system and the determination of oceanic surface density, *J. Phys. Oceanogr.*, *14*, 1159–1171, 1984.

Semtner, A. J., and Y. Mintz, Numerical simulation of the Gulf Stream and mid-ocean eddies, *J. Phys. Oceanogr.*, *7*, 208–230, 1977.

Thompson, J. D., and W. J. Schmitz, A limited area model of the Gulf Stream: Design, initial experiments, and model-data intercomparison, *J. Phys. Oceanogr.*, *19*, 791–814, 1989.

Veronis, G., Model of world ocean circulation, III, Thermally and wind driven, *J. Mar. Res.*, *36*, 1–44, 1978.

S. S. Drijfhout, Royal Netherlands Meteorological Institute, P.O. Box 201, 3730 AE De Bilt, Netherlands. (e-mail: drijfhout@knmi.nl)

(Received November 15, 1993; revised April 29, 1994; accepted May 13, 1994.)